RESEARCH ARTICLE
doi: 10.2306/scienceasia1513-1874.2022.035

ScienceAsia 48 (2022): **287–293**

Hyperspectral remote sensing estimation of soil nutrients in the black soil region based on computer vision model

Li Ma[a], **Anqi Li**[a], **Helong Yu**[a,b], **Guifen Chen**[c,*]

[a] Information and Technology College, Jilin Agricultural University, Changchun 130118 China
[b] Jilin Agricultural University Wisdom Agriculture Research Institute, Changchun 130118 China
[c] Changchun College of Humanities, Changchun 130000 China

*Corresponding author, e-mail: chenguifen@jlau.edu.cn

Received 26 Feb 2021, Accepted 23 Nov 2021
Available online 28 Feb 2022

ABSTRACT: With the continuous development of modern agriculture, precision fertilization is based on the profit and loss of soil moisture and nutrients, scientific irrigation and formula fertilization, to achieve full resource efficiency. Hyperspectral remote sensing and computer vision technology are very important tools in precision fertilization. The purpose of this study was to estimate soil nutrients in the black soil region using computer vision technology combined with hyperspectral remote sensing. Soil samples (n=163) were collected from northwestern China. The content of soil organic matter (SOM), total nitrogen (N), phosphorus (P), potassium (K), and pH were measured. In the study, measured nutrient component spectrum conversion data was selected to compare global and local spatial autocorrelation of the soil nutrient elements. Multi-step regression analysis was used to estimate soil nutrients. Finally, the estimated value was compared with the actual value, and the percentage error was calculated to evaluate accuracy. The results showed that the prediction model of soil total nitrogen content was the most correct, with a prediction accuracy of 78.16% and a relative error of 21.84%, It is concluded that computer vision hyperspectral remote sensing has high estimation accuracy and effective reflection. This study provides a basis for the determination of soil nutrients estimated by remote sensing and can supplement the implementation of precise fertilization.

KEYWORDS: computer vision, soil nutrient, hyperspectral data, remote sensing, precision fertilization

INTRODUCTION

Soil composition is one of the most important limiting factors affecting crop growth [1]. Crops need to obtain water and nutrients from farmland soil. Traditional soil testing and analysis rely on laboratory chemical analysis, which is not only complex and time-consuming, but also high cost, which is not conducive to a large-scale and accurate understanding of soil fertility information and distribution [2]. In hyperspectral data, each pixel is composed of different ground object spectra. The amount of data is considerable and the data information is very rich. This enabled us to restore ground feature details via hyperspectral data. Hyperspectral remote sensing data has the advantage of high spectral resolution compared to multispectral remote sensing data, which makes it easier to solve problems that cannot be solved by a multispectral data field. Hyperspectral remote sensing plays an important role in the social economy, national defense and military affairs [3, 4].

In the early 20th century, hyperspectral remote sensing technology was used to carry out applied research and monitoring of soil information, which showed a clear correlation between soil nutrient content and the soil reflectance spectrum. Bendor et al [5] projected six soil indexes, including carbonate, by analyzing soil in the near-infrared spectrum, and predicted Fe, A1, Mg in montmorillonite via near-infrared analysis. Chodak et al [6] studied the relationship between biochemical substances in forest soil by linear regression analysis. Zhao et al [7] evaluated the total nitrogen content in loess areas of China using near infrared spectroscopy. Song et al [8] predicted SOM and pH levels in soil, following derivative treatment, with near infrared spectroscopy, and the correlation coefficient was greater than 0.8. Li et al [9] predicted the content of alkali-hydrolyzable nitrogen in soil also via near infrared spectroscopy. Li et al [10] found that there was a good correlation between nIR spectrum and soil nutrients, and it was feasible to estimate soil organic matter and pH using NIR spectrum. There are many studies on the estimation of soil physicochemical parameters at home and abroad [11–13], but when these models are applied to other fields, relatively large errors result. Most previous research has analyzed the relationship between spectral transformation form and soil nutrient content and established quantitative estimation regression models. Spectral data processing is simple but lacks in depth mining and soil spectral information application, negatively affecting model estimation accuracy, and comparative analysis of the data processing system.

The main algorithms used in this study are semivariance function and spatial autocorrelation analysis. Combined with experimental data, comparative analysis was conducted from the following three aspects: hyperspectral remote sensing model estimation, the prediction and estimation analysis of soil content via computer vision hyperspectral remote sensing model,

and the spectral characteristics of soil with different nutrient content.

MATERIALS AND METHODS

Experimental materials and treatment

Data collection

The soil samples were collected from Guanzhong and all collected soil samples were promptly returned to the laboratory. The samples were then dispersed as much as possible in order to have the widest possible range of nutrient content in the sample cover. Other soil samples taken from each sampling point were packaged separately without mixing. The soil was simply shielded so that our experiments were as close as possible to field measurements. A total of 163 samples were collected and sealed in plastic bags in the laboratory for chemical analysis and spectrum collection.

After the soil samples are returned to the laboratory, drying, grinding, passing through 2 mm nylon screen, sealing and storing, for heavy metal determination. Soil test and analysis was then conducted according to "Technical Specifications for Soil Analysis" [14].

Experimental spectrometry

Spectral measurements were taken in a dark room with controlled lighting conditions. The samples were placed in a sample dish with a 12 cm diameter and 1.8 cm depth (optically infinitely thick soil sample depth of 1.5 cm). The surface of the samples was flattened with a ruler. Light was provided by a 1000 W halogen lamp, 70 cm from the soil sample surface, and with a zenith angle of 30°. A sensor probe with 80° field of view was placed vertically above the soil sample, 15 cm from the surface. We used a 2.1 cm diameter circular probe receiving spectrum, to obtain the soil reflection spectrum.

Computer vision and hyperspectral remote sensing estimation

Preprocessing methods of hyperspectral data

Spectral pre-treatment has a significant impact on model prediction accuracy [15]. Different methods have varying degrees of success in removing noise, reducing errors, and extracting valid spectral information. Experiments were conducted to optimize the appropriate spectral pretreatment method [16].

(1) *Smoothing.* The purpose of smoothing is to eliminate high frequency random errors and improve the signal-to-noise ratio of the analytic signal. Commonly used signal smoothing methods include moving average convolution smoothing, fast Fourier transform (FFT), wavelet demonizing, and Kalman filtering. When a moving average method is used, it is very important to select the smoothing window width. Currently, there is no fixed method to determine the smooth window width, which needs to be verified several times. In this method, the least square fitting coefficient is used as the corresponding function of digital filtering to convolute and smooth the original spectrum [17, 18].

(2) *Differential.* The first and second derivatives can eliminate baseline drift, strengthen the spectral band characteristics, and overcome the spectral band overlap. They are widely used in baseline correction and spectral resolution pre-processing in near-infrared spectroscopy analysis. The higher the differential order, the narrower the differential peak width was. Differential spectra with narrow peak widths have a stronger emphasis on absorption [19]. For some peaks with a mutual interference effect, the differential spectrum also has the following effects.

When the peaks are close to each other and the spectrum appears as a single peak, the differential spectrum separates the peaks. For the small peaks hidden in the wide absorption band with strong absorption, the differential spectrum has an effect [20]. The differential spectrum plays an important role, and has an obvious influence on the baseline change. The first-order differential removes the wavelength independent drift and the second-order differential removes the wavelength dependent drift. This characteristic is effective in eliminating the rising trend caused by water absorption in near infrared spectroscopy [21].

(3) *Variable standardization.* Variable standardization (SNV) correction can be used to correct spectral errors due to scattering between samples. According to SNV correction, the absorbance values at each wavelength point in each spectrum should satisfy a certain distribution [22]. Therefore, it is not necessary to calibrate each spectrum with an "ideal" spectrum. The SNV is the original spectrum minus the mean of the spectrum, divided by the standard deviation of the spectral data, which essentially normalizes the original spectral data [23].

The mean value of the normalized spectral data is 0 with a standard deviation of 1. Since SNV correction is only used to eliminate the effects of linear shifts in the sample spectrum, the spectral data must also be expressed as a function. As a highly practical spectral data pre-processing method, SNV is widely used in solid sample reflection spectral data preprocessing [24].

The change trends of the spatial autocorrelation characteristics of soil nutrient indicators with spatial distance are discussed. Additionally, the characteristics of Moran's I in different directions with spatial distance is analyzed. In order to reveal the spatial relationship of the research object geographical location, it is necessary to first define the adjacency relationship of

spatial objects. The first step in spatial autocorrelation analysis is to establish the normalized spatial weight matrix $W_{(n\times n)}$ to represent the location relationship of soil samples in the study area.

$$W = \begin{bmatrix} w_{11} & w_{12} & \cdots & w_{1n} \\ w_{21} & w_{22} & \cdots & w_{2n} \\ \vdots & \vdots & \vdots & \vdots \\ w_{n1} & w_{n2} & \cdots & w_{nn} \end{bmatrix} \tag{1}$$

where w_{ij} represents the degree of adjacency between sample i and sample j in the region. For the small-scale spatial autocorrelation analysis of small watersheds in the black soil region, the k-nearest weight matrix is used to ensure that each object has k neighbors. When region j belongs to one of the nearest k neighbors of region i, w_{ij} is 1, otherwise it is 0. The global Moran's I is I, and the formula is as follows:

$$I = \begin{cases} n\sum\limits_{1}^{n}\sum\limits_{j=1}^{n} w_{ij}(x_i - x)(x_j - x) \\ \left(\sum\limits_{i=1}^{n}\sum\limits_{j=1}^{n} w_{ij}\right)\sum\limits_{i=1}^{n}(x_i - x)^2 \end{cases} \tag{2}$$

where n is the number of spatial data; x_i and x_j are the attributed values of spatial elements in zone i and zone j respectively; x is the average value of all spatial data; w_{ij} is the element of spatial weight matrix, which is generally a symmetric matrix where $w_{ij} = 0$. For global Moran's I, the significance level of spatial autocorrelation of spatial elements is generally tested using the standardized statistic $Z(I)$:

$$Z(i) = \begin{cases} I - \mathrm{E}(I) \\ \mathrm{Var}(I) \end{cases} \tag{3}$$

where $\mathrm{Var}(I)$ and $\mathrm{E}(I)$ are Moran's I theoretical variance and the theoretical expectation of I, respectively. The inference of Moran index is based on a random sequence. It recalculates the statistics multiple times to produce a reference distribution. By comparing the comparison statistics with the reference analysis, the significance level of the spatial autocorrelation of soil nutrient elements in the study area can be investigated.

Hyperspectral image classificationprocess

In remote sensing images, similar types of ground objects have consistent or similar characteristics. Based on this, remote sensing image classification technology is becoming highly-developed. Remote sensing image classification is based on the similarity of pixel features to isolate different features [25]. In remote sensing image classification studies, the role of hyperspectral image classification is self-evident. According to whether a priori condition is required for classification, hyperspectral image classification algorithms can be divided into either supervised classification or unsupervised classification [26].

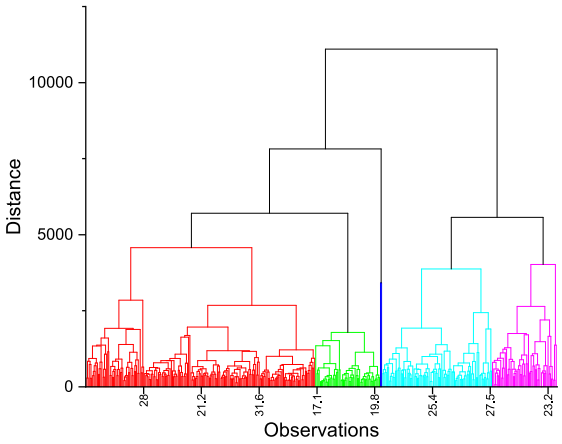

Fig. 1 Clustering iterative process of SOM.

The principle of the algorithm is to adopt the centers of several clusters, with each center representing a category. According to a specific measurement method, the samples are separated into the center of each cluster to form a preliminary classification state. Subsequently, discriminant rules are used to determine whether the classification is correct, and if not, iterative division continues until it is correct [27, 28].

Take SOC as an example. Set the number of clusters to 5, and the lower limit of the distance between starting centers is 6429.972. Repeatedly adjust the distribution of each data point and carry out iterations. After 18 iterations, the cluster centers are constant. The iterative change process of the cluster centers is shown in Fig. 1.

Variation characteristics

The semi-variance function obtains the continuous model by fitting the sample data. The fitting effect and spatial dependence of each nutrient element in the soil at any spatial distance are determined by the semivariance function model parameters [29]. The nugget value represents the sampling error and the variation within the minimum sampling distance, and the base value represents the total variation of the index at the current scale. The maximum fitting coefficient and least square sum of the fitting residuals can be used to evaluate the fitting effect of the variogram model [30]. The ratio of nugget value to abutment value is the spatial heterogeneity ratio, which indicates variability on a regional scale. This parameter judges the degree and scale of the indicators' spatial variation and the rest of the variation is system variation. The number of study area sample points and model fitting effect are different, and the spatial position of sample points within the study area also affects the fitting effect [31].

Spatial autocorrelation analysis

Spatial autocorrelation analysis is a type of spatial statistical method, generally used to reveal the structural form and spatial aggregation characteristics of spatial variables. According to this method, the global and local spatial autocorrelations of soil nutrient element indicators in the study area were carried out. Spatial autocorrelation analysis is also an important indicator when testing the correlation between the attribute values of each index and the points on their adjacent spatial positions. Moran's I index is a commonly used spatial autocorrelation indicator. If Moran's I index is $>$ 0, it indicates that the point has an equivalent change trend with points in its adjacent space, indicating that the spatial phenomenon has clustering. When Moran's I index is less than 0, the opposite is true.

(1) *Global spatial autocorrelation analysis.* Global spatial autocorrelation is a statistic that describes whether there are spatial aggregation characteristics of geographical spatial elements on an overall scale. The variance trend in the spatial autocorrelation characteristics of soil nutrient indicators with spatial distance is discussed. Additionally, the characteristics of Moran's I in different directions with spatial distance are analyzed. In order to reveal the spatial relationship of the research object geographical location it is necessary to define the adjacency relationship of spatial objects. The first step in spatial autocorrelation analysis is to establish the normalized spatial weight matrix $W_{(n\times n)}$ to represent the location relationship of soil samples within the study area.

(2) *Local spatial autocorrelation analysis.* To ascertain the soil pH and water content in significant global spatial autocorrelation, the spatial autocorrelation of the research object at 0°, 45°, 90° and 135° was analyzed. This can further quantify the degree of difference and significance between specific spatial elements and surrounding elements.

Multiple stepwise regression quantitative estimation

The selected spectral conversion data was analyzed via multi-step regression with soil. As a result, (1/lgr) showed the best fitting effect on the premise that the band selected by multicollinearity elimination and significance test was removed. The maximum values of the coefficient of determination RPD (Residual Predictive Deviation) were 0.51 and 1.41, respectively, and the minimum RMSEC (Root Mean Square Error of Calibration) was 6.28. The model proved to have rough stability and estimation ability. The other 11 model groups had little variation in estimation ability, and coefficient of determination $<$ 0.5, in the range 0.42 to 0.47, RPD in the range 1.31 to 1.37, and the number of selected bands in the range 3–5.

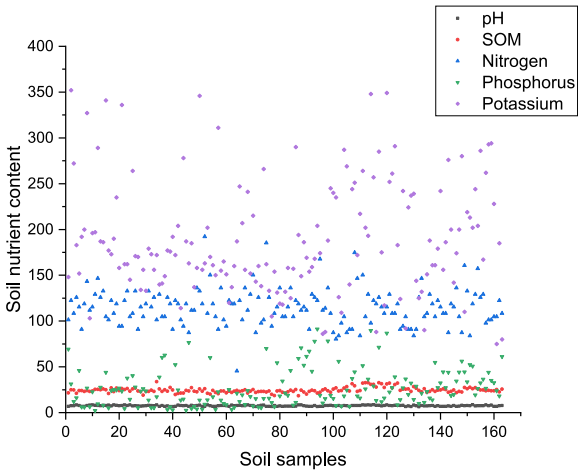

Fig. 2 Soil nutrient content.

Table 1 Statistical characteristics of soil nutrients and conventional elements.

Element	Min (g/kg)	Max (g/kg)	Average (g/kg)	Standard deviation	Coefficient of variation (%)
C:N	8.07	23.49	12.25	3.55	28.98
SOM	7.49	32.75	27.93	6.85	24.53
pH	6.91	9.00	8.08	0.43	5.32
Al	44.67	77.64	61.34	7.62	12.42
Fe	15.64	49.77	32.07	6.31	19.68
Mg	6.37	20.08	10.16	2.27	22.34
Si	194.81	331.66	272.64	23.88	8.76
Mn	0.28	1.54	0.69	0.20	28.99

RESULTS AND DISCUSSION

Statistics of soil nutrient content in the black soil area

Based on traditional statistical theory, the soil properties of 163 valid samples were analyzed, including maximum, minimum, average, and standard deviation, and coefficient of variation. Soil nutrient content is shown in Fig. 2.

The coefficient of variation in Table 1 can be used to measure the spatial variation intensity of soil properties. Generally, the variation coefficient is considered small in the range of 0–10%, moderate in the range of 10–100%, and highly variable over 100%. It can be seen from the table that apart from a small variation in soil Si and pH value, the remaining soil composition was determined as medium variation, and the coefficient of variation of soil nutrient composition, total carbon and carbon-nitrogen ratio were larger than that of conventional soil elements. This is possibly due to both human activities and natural factors. There is a resulting loss of nutrients and altered ratio of total carbon and carbon to nitrogen in some areas, which affects the distribution of soil nutrients and the total carbon and carbon-nitrogen ratio [32, 33]. The main

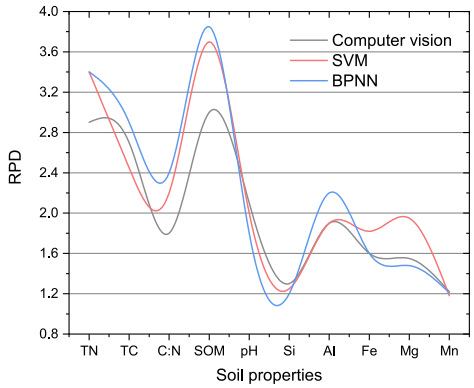

Fig. 3 RPD comparison of model validation.

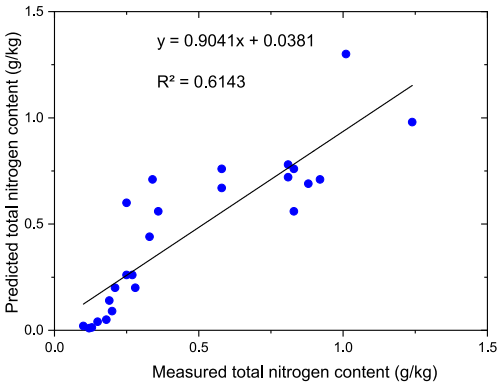

Fig. 4 Correlation between predicted and measured values of soil total nitrogen content.

factor in the moderate variability of soil conventional elements in the study area is animal husbandry, with human activities exhibiting a lesser effect [34]. The variability of soil conventional elements is greatly affected by structural factors such as topography, parent material, and climate [35, 36]. These conventional elements are the basic elements of minerals, so variability is low.

Comparison of hyperspectral remote sensing model estimation results

The results of the optimum model for estimating soil properties in the full band of soil visible near infrared spectroscopy. Computer vision technology, BPNN (Back-Propagation Neural Network) and SVM were compared longitudinally, and the RPD comparison was verified by the best estimation models of 10 types of soil characteristic content, as shown in Fig. 3.

It can be seen from Fig. 3 that three computer vision technology models, along with BPNN and SVM can be used to estimate soil TN, TC, C:N, SOM, pH, Al, Fe and Mg, but not Si and Mn. The BPNN model lacks the ability to estimate Si and Mn elements, while computer vision technology and SVM can do so approximately. It is evident that spectral estimation models constructed by these three methods are applicable for most soil properties in this study area [37].

After comparing the accuracy of the three models, there were 4 BPNN models with RPD $\geqslant 2$, 7 with $1.4 \leqslant$ RPD < 2, and 6 with RPD < 1.4; 4 with RPD $\geqslant 2$, 9 with $1.4 \leqslant$ RPD < 2, and 4 with RPD < 1.4; 5 with RPD $\geqslant 2$ by computer vision technology. In conclusion, the accuracy of the computer vision technology model was equivalent to the SVM model, but the number of computer vision technology models with precision RPD $\geqslant 2$ was one more than SVM model. The worst performing model was BPNN, and the model precision of RPD < 1.4 was 6. BPNN is a classical model that deals with linear problems, while SVM and computer vision technology are better at solving nonlinear problems.

Table 2 Validation of model for predicting soil characteristic parameters.

Characteristic parameter	Predicted value	Measured value	Relative error	Prediction accuracy
TN (g/kg)	0.58	0.65	21.88	78.16
TP (g/kg)	1.03	1.13	24.31	75.64
TK (g/kg)	21.74	19.39	29.72	70.28

Prediction and estimation of soil content based on the computer vision hyperspectral remote sensing model

In order to verify the accuracy of the above models in estimating main nutrient content and real-time monitoring values, the soil total nitrogen, total phosphorus and total potassium content estimated by spectra were compared to the measured values of 25 samples corresponding to field synchronous measurement, as shown in Fig. 4. We then examined the correlation between the predicted and measured values of soil total nitrogen content.

According to Fig. 4, through the analysis and comparison of the predicted and measured values of soil total nitrogen content, it was concluded that a correlation did exist, and the determination coefficient $R^2 = 0.6143$. The validation of the model for predicting soil characteristic parameters is shown in Table 2.

It can be seen from Table 2 that the prediction accuracy of the model refers to its fitting degree, that is, the integrity of the fitting degree between the simulated actual values generated by the prediction model. Prediction accuracy is an important indicator in ascertaining whether the prediction method is applicable to the predicted object. The relative error reflects the credibility of the prediction results [38].

Spectral characteristics of soil with different nutrient content

Soil is the main source of nutrients needed for crop growth. Therefore, it is necessary to consistently judge

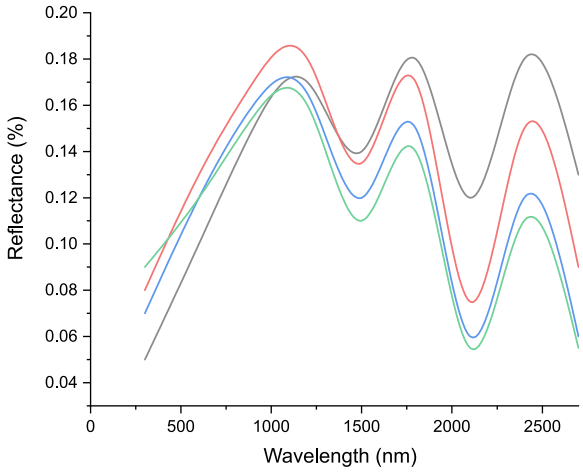

Fig. 5 Spectral curves of soils with different N, P and K contents.

soil nutritional status, and provide scientific guidance for the application of fertilizer. The results of the soil hyperspectral test and the varying increases in N, P and K content show that the N, P and K content soil spectral curves initially increase and then decrease within the entire frequency band (350–2500 nm). With the presence of N, P and K in soil, the spectral reflectance of soil decreases, and there is a good negative correlation between the soil nutrient elements and spectral reflectance. Therefore, it is feasible to use hyperspectral reflectance to study and explain the content of nitrogen, phosphorus and potassium in soil, which has potential application value. Fig. 5 shows the spectral curves of soils with different N, P and K content.

Typical spectral soil characteristics are analyzed in Fig. 5. The variation in visible and near-infrared regions is relatively mild, without obvious peaks and valleys. It increases slowly between 350–800 nm to form a slanted line, and the spectral reflectance increases with increases in wavelength. Within the band 800–2500 nm, the spectral curve tends to be gentle, and the reflectance changes slightly between 0.25–0.28. The results show that there are absorption characteristics at 1300 nm, 1700 nm and 2167 nm, and there are obvious water vapor absorption bands near 1400 nm, 1800 nm and 2400 nm. All soil spectral curves close to the shortwave direction, and most soil spectral reflectance, are not high up in the visible light range, and there is a strong positive correlation between the bands [39].

The results show that the spectral reflectance of different soil textures varies. For soil composed of finer particles, the spectral curve is smoother with a higher reflectance; while in coarser soil, the spectral curve fluctuates significantly, especially at 1300 nm, 1800 nm and 2200 nm [40].

CONCLUSION

The relationship between soil spectral characteristics and soil spectral properties cannot be estimated by a simple SVM model. Although the estimation ability of the computer vision technology model and SVM model is similar, the estimation accuracy of the computer vision technology model is higher overall. This is because the SVM model falls easily into the local minimum value and appears to over fit. Computer vision technology can solve small sample problems, over fitting, and high-dimensional pattern recognition. Consequently, it possesses the best model estimation ability.

It was feasible to predict soil total nitrogen by eliminating the influence of soil type and other factors on the spectrum through mathematical methods. The results show that there is a nonlinear relationship between the spectrum and total phosphorus content, and the computer vision method has outstanding nonlinear mapping ability. It is reasonable to predict the soil type after already determining it. Our results were consistent with those of other studies.

The comparison of the accuracy of the computer vision, BPNN and SVM models in estimating the contents of all spectral bands and 10 types of soil properties showed the computer vision model has the best estimation ability. The SVM model took second place, and the BPNN model had the lowest estimation ability. Therefore, the BPNN model has some limitations with estimation, while the SVM and computer vision models can better deal with the nonlinear relationship between spectrum and soil properties.

Acknowledgements: This work was supported by the National Natural Science Foundation of China–Joint Fund (u19a2061), Jilin Provincial Department of Education Project (No. JJKH20210336KJ), Jilin Province Ecological Environment Department Project (2021-07), Jilin province science and technology development plan project (No. 20190301024NY, 20200403176SF, 20200301047RQ).

REFERENCES

1. Li WX, Zhang FY, Cui GH, Wang YY, Cheng HC, Liu HW, Zhang LP (2021) Effects of bio-organic fertilizer on soil fertility, microbial community composition, and potato growth. *ScienceAsia* **47**, 347–356.
2. Wang J, Tiyip T, Ding J, Liu W (2016) Estimation of desert soil organic carbon content based on hyperspectral data preprocessing with fractional differential. *Agric Eng* **32**, 161–169.
3. He T, Wang J, Lin ZJ, Cheng Y (2009) Spectral features of soil organic matter. *Geo Spat Inf Sci* **12**, 33–40.
4. Liu HJ, Pan Y, Dou X, Zhang XL, Qiu ZC, Xu MY, Xie YH, Wang N (2018) Soil organic matter content inversion model with remote sensing image in field scale of black soil area. *Agric Eng* **34**, 127–133.
5. Bendor E, Banin A (1995) Near-infrared analysis as a rapid method to simultaneously evaluate several soil properties. *Soil Sci Soc Am J* **59**, 364–372.

6. Chodak M, Ludwig B, Khanna P, Beese F (2015) Use of near infrared spectroscopy to determine biologi-cal and chemical characteristics of organic layers under spruce and beech stands. *J Plant Nutr Soil Sci* **165**, 27–33.
7. Zhao SL, Peng YK (2002) Analysis of soil moisture, organic matter and total nitrogen content in loess in China with near infrared spectroscopy. *Zhongguo Wuji Fenxi Huaxue* **30**, 978–980.
8. Song HY (2005) Simulation of soil and crop information and their relationship based on spectral techniques. PhD thesis, Zhejiang Univ, China. [in Chinese]
9. Li W, Zhang SH, Zhang Q, Zhang SQ (2007) Rapid prediction of available N, P and K content in soil using near-infrared reflectance spectroscopy. *Nongye Gongcheng Xuebao* **23**, 55–59.
10. Li YF, Wang DC, Zhang DY, Zhu DZ (2012) The detection of soil parameters by portable near infrared spectrometer. *Appl Mech Mater* **128–129**, 718–726.
11. Bendor E, Chabrillat S, Demattê J (2009) Using imaging spectroscopy to study soil properties. *Remote Sens Environ* **113**, 38–55.
12. Moreira Scafutto RD, Roberto D, De Oliveira WJ (2017) Hyperspectral remote sensing detection of petroleum hydrocarbons in mixtures with mineral substrates: Implications for onshore exploration and monitoring. *ISPRS J Photogramm* **128**, 146–157.
13. An D, Zhao G, Chang C (2016) Hyperspectral field estimation and remote-sensing inversion of salt content in coastal saline soils of the Yellow River Delta. *Int J Remote Sens* **37**, 455–470.
14. Du S (2016) *Technical Specifications for Soil Analysis*, 2nd edn, China Agricultural Press, Beijing.
15. Chen JG, Chen J, Wang QJ, Zhang Y, Ding HF, Huang Z (2016) Retrieval of soil dispersion using hyperspectral remote sensing. *Spectrosc Spect Anal* **44**, 563–572.
16. Xie XY, Liu YM, Li JZ, Wei C, Ling W (2016) Remote sensing estimation of plant litter cover based on the spectra of plant litter-soil mixed scenes. *Guangpuxue Yu Guangpu Fenxi* **36**, 2217–2223.
17. El-Sharkawy M, Sheta A, El-Wahed M, Arafat S, Behiery O (2016) Precision agriculture using remote sensing and GIS for peanut crop production in arid land. *Int J Plant Soil Sci* **10**, 1–9.
18. Kozoderov VV , Dmitriev EV (2018) Models of pattern eecognition and forest state estimation based on hyperspectral remote sensing Ddata. *Izv Atmos Ocean Phys* **54**, 1291–1302.
19. Zhang C, Qin Q, Chen L, Wang N, Bai Y, Zhao S (2017) Hyperspectral remote sensing for coal-bed methane exploration. *J Mines Met Fuels* **65**, 115–117.
20. Ye C, Li Y, Cui P (2020) Landslide detection of hyperspectral remote sensing data based on deep learning with constrains. *IEEE J Stars* **99**, 1–14.
21. Viana OH, Mercante E, Andrade MGD, Felipetto H, MAV Boas (2018) Potential of hyperspectral remote sensing to estimate the yield of a *Crambe abyssinica* Hochst crop. *J Appl Remote Sens* **12**, 16023–16021.
22. Bioucas-Dias JM, Plaza A, Camps-Valls G, Scheunders P, Nasrabadi N, Chanussot J (2013) Hyperspectral remote sensing data analysis and future challenges. *IEEE Geosci Remote Sens Mag* **1**, 6–36.
23. Xia J, Chanussot J, Du P, He X (2016) Rotation-based support vectormachine ensemble in classification of hyperspectral data with limited training samples. *IEEE T Geosci Remote* **54**, 1519–1531.
24. Li Z, Guo X (2018) Non-photosynthetic vegetation biomass estimation in semiarid Canadian mixed grasslands using ground hyperspectral data, Landsat 8 OLI, and Sentinel-2 images. *Int J Remote Sens* **39**, 6893–6913.
25. Sharififar A, Singh K, Jones E, Ginting FI, Minasny B (2019) Evaluating a low-cost portable nir spectrometer for the prediction of soil organic and total carbon using different calibration models. *Soil Use Manage* **12**, 607–616.
26. Zheng Y, Li J, Shang R, Hou B, Zhang X (2016) Local collaborative representation with adaptive dictionary selection for hyperspectral image classification. *IEEE Geosci Remote S* **13**, 1482–1486.
27. Zhang X, Liang Y, Chen L, Ning H, JiaoL, Zhou H (2017) Recursive autoencoders-based unsupervised feature learning for hyperspectral image classification. *IEEE Geosci Remote S* **99**, 1928–1932.
28. He W, Zhang H, Zhang L (2017) Weighted sparse graph based dimensionality reduction for hyperspectral images. *IEEE Geosci Remote S* **13**, 686–690.
29. Meng J, Cheng Z (2020) Improving the estimation of soil-available nutrients at the sub-field scale using time-series UAV observations. *Remote Sens Lett* **11**, 739–747.
30. Szparaga A, Ewa Czerwińska, Tomkiewicz D (2017) Assessment of plant germination intensity with the use of automated system with computer vision method. *Nephron Clin Pract* **21**, 83–91.
31. Sutcliffe M, Lewis J (2016) Automatic defect recognition of single-v welds using full matrix capture data, computer vision and multi-layer perceptron artificial neural networks. *Insight* **58**, 487–493.
32. Bosch OJ, Revilla M, Paura E (2019) Answering mobile surveys with images: An exploration using a computer vision API. *Soc Sci Comput Rev* **37**, 669–683.
33. Chen GF, Ma L, Chen H (2013) Research status and development trend of precision fertilization technology. *J Jilin Agric Univ* **35**, 253–259. [in Chinese]
34. Wang Z, Xu L, Zhang S (2002) Corresponding relationship between soil trace elements and human activity intensity. *Soil Sci* **4**, 303–305. [in Chinese]
35. Waeldchen J, Maeder P (2018) Plant species identification using computer vision techniques: A systematic literature review. *Arch Comput Methods Eng* **25**, 507–543.
36. Naik N, Raskar R, Hidalgo CA (2016) Cities are physical too: Using computer vision to measure the quality and impact of urban appearance. *Am Econ Rev* **106**, 128–132.
37. Li D, Yang F, Wang X (2017) Study on ensemble crop information extraction of remote sensing images based on SVM and BPNN. *J Indian Soc Remote Sens* **45**, 229–237.
38. Sun T, Yang CH, Zhu HQ, Li YG, Chen JM (2019) A wavelength selection method of UV-Vis based on variable stability and credibility. *Spectrosc Spect Anal* **39**, 3438–3445.
39. Anne N, Abd-Elrahman AH, Lewis DB, Hewitt NA (2014) Modeling soil parameters using hyperspectral image reflectance in subtropical coastal wetlands. *Int J Appl Earth Obs* **33**, 47–56.
40. Li XY, Fan PP, Hou GL, Lü MR, Liu Y (2017) Visible-near infrared spectrum of soil nutrient rapid detection. *Spectrosc Spect Anal* **37**, 3562–3566.